EVIDENCE FOR HIGHLY VARIABLE, PRE-ACCRETIONARY OXIDATION OF GEMS. Z. Gainsforth[1,†], A. L. Butterworth[1], C. E. Jilly-Rehak[1], A. J. Westphal[1], [1]Space Sciences Laboratory, University of California, Berkeley, CA 94720, [†]e-mail: zackg@ssl.berkeley.edu.

Introduction: Recent work on GEMS has shown that they are chemically and texturally diverse and have experienced a variety of formation or alteration conditions. Sulfidation and heating of GEMS-like objects can form igneous textures between the embedded metals and sulfides [1, 2]. Low temperature aggregation in the nebula can cement GEMS into clumps bound to each other [3, 4]. Heating of GEMS in the nebula can lead to equilibrated aggregates [5] or heating during atmospheric entry can produce altered aggregates [6]. Recent work comparing GEMS in IDPs to interstellar material showed that it is difficult to reconcile the oxidation state and particle size distributions of Fe-bearing objects in the ISM with the properties of GEMS [7]. Understanding the oxidation processes active in the nebula and being able to distinguish them from atmospheric entry is of high importance.

Experimental: We studied GEMS from a cluster IDP (L2071, 17) which contains some evidence for oxidation of phases during atmospheric capture but retains a large fraction of relatively primitive material. We used an FEI Titan Transmission Electron Microscope (TEM) located at the National Center for Electron Microscopy at the Lawrence Berkeley National Laboratory. We used beam voltages between 80-200 keV for imaging and electron diffraction. A 0.6 sr EDS detector provided elemental mapping and enabled EDS tomography. We used a combination of ultramicrotomy and Focused Ion Beam (FIB) preparation — the latter providing better petrographic context at the expense of losing material.

Observations: We analyzed several dozen GEMS from seven different CP-IDPs from the same cluster. Here we focus on two GEMS aggregates, the first from an ultramictomed section, and the second from a FIB section.

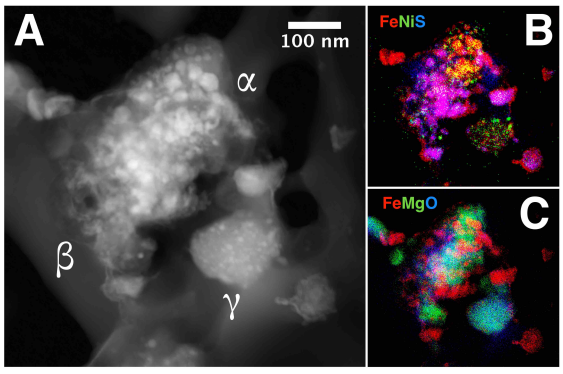

Figure 1: (A) STEM HAADF image of a GEMS aggregate showing three GEMS with varying oxidation. (B) EDS map with Fe (red), Ni (green), S (blue) shows an Fe-Ni metal rich subunit (α), a sulfide-rich subunit (β), and a Ni-metal rich subunit (γ). (C) EDS map with Fe (red), Mg (green), O (blue) shows that the three subunits have different Mg and O contents.

Microtomed: Figure 1A shows a STEM image of an ultramicrotomed GEMS aggregate from L2071, 17, particle 3, and EDS maps in 1B, C show that the aggregate consists of three GEMS with varying characteristics. GEMS α is a typical GEMS with embedded nanometals, an Mg-rich core, and some sulfide and carbon around the periphery. Fe/Ni=13, which is near the chondritic value of 20. The GEMS also contains detectable P, K and Zn, at a few hundred ppm each. GEMS β is a sulfide-rich GEMS with a number of sulfides decorating the periphery of the GEMS. Fe/Ni=24 which is also close to the chondritic value, and the GEMS contains detectable Na, P, K and Zn. GEMS γ is a Fe-poor GEMS consisting of Ni metals and several $\approx$ 10 nm sulfides on its surface. Fe/Ni=5, which is substantially lower the other two GEMS. Na, P, K are all in the hundreds of ppm range. Tomography shows that sulfides are present only on the outside of each GEMS, and that metal grains are on the inside. A faint magnetite rim about 10 nm thick can be seen running along the upper right and lower left edges of the aggregate as an Fe-rich, S-poor line and as an Fe-rich rim around some of the larger sulfides. However, most of the material does not contain magnetite.

FIBed: We FIBed another CP-IDP from the same cluster (L2071, 17) named Dumpty. Dumpty contains a GEMS aggregate about 2 μm across with about 20 GEMS in the FIB section (Figure 2). The aggregate comprises several sub-aggregates (regions) which are attached to each other with carbonaceous material labeled α through η. The regions each comprise several GEMS attached to each other in some cases with carbonaceous material, and in other cases by apparent sintering.

$\alpha, \beta, \gamma, \epsilon$ and ζ are GEMS regions, while δ and η are filled primarily with equilibrated aggregates — though a few GEMS are present. η is dominated by carbonaceous material and sulfides, and is bounded on the lower side by a Fo_{80} olivine.

Ca is present at 1 at% or below in all the regions except for δ where Ca is present at 3 at%. K is present at 0.1 at% in δ, ζ, and η while it was not detected in the rest of the aggregate.

The GEMS at the top of δ, marked with the arrow, is also noteworthy since the metal is Ni-rich as seen in the GEMS within Figure 1, yet is surrounded by sulfides with little to no magnetite. The GEMS in ζ and ϵ are also Ni-rich. Small Ni-rich metals are present throughout all the GEMS in the aggregate.

The carbonaceous material between and within the regions is rich in N indicating it is primitive nebular carbon and not simply deposited by the FIB process. The presence of N also indicates that the FIB process did not substantially damage the material within the IDP.

Discussion: In Figure 1 the three GEMS apparently record a diverse history of oxidation. Since the Fe-FeO buffer lies several log units below the Ni-NiO buffer, the loss of Fe in γ appears to record a more oxidizing environment than α and β. The small sulfides on the outside of γ do not have enough

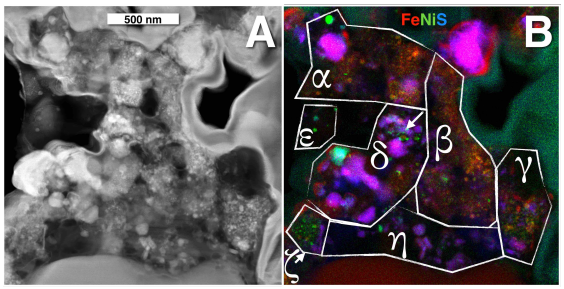

Figure 2: (A) STEM HAADF image of an aggregate of GEMS aggregates. (B) EDS map with Fe (red), Ni (green), S (blue) showing regions within the larger GEMS aggregate.

volume to account for the overall deficit of Fe and S. Therefore, either the GEMS formed originally with Ni-rich metals, which may imply formation below Ni-NiO but near or only slightly below Fe-FeO, or it experienced subsequent oxidation that enriched the Ni-content of the metal after formation. Since the atmospheric abundance of sulfur is < 1 ppm [9], $f_{S_2} < f_{O_2}$ by several log units. However, sulfides would only be stable in the presence of the magnetite that we observe when $f_{S_2} > f_{O_2}$ by $\approx$ 20 log units [10]. Therefore, if oxidation from atmospheric entry were sufficient to oxidize the GEMS, then it should also have converted the nanosulfides on the surface to magnetite. We are left with three scenarios: 1) The GEMS formed in an Fe-poor or Ni-rich environment. 2) The GEMS formed in a high oxygen fugacity environment, or 3) the GEMS was oxidized after formation, but in the nebula.

Comparing α and β shows a difference in the sulfur fugacity (f_{S_2}). While α contains Fe-Ni metals and only a few sulfides on its periphery, β contains fewer metals within its core, but many sulfides around the periphery. This hints at different formation origins for the GEMS in this aggregate; a datum also evidenced by the FIBed sample, Dumpty.

The large aggregate of GEMS from Dumpty (Figure 2) also allows us to see that oxidative processes were active in the nebula. The GEMS at the top of δ, marked by an arrow in Figure 2B, has Ni-rich metals and abundant sulfides. The presence of sulfide without magnetite indicates that the GEMS was not oxidized by atmospheric entry.

It has been shown that equilibrated aggregates can be formed by heating of GEMS [8], so it is possible that the GEMS in δ was oxidized at the same time that the rest of δ was heated, but did not equilibrate with the rest of the material since the process occurred in disequilibrium. However, the high Ca and K in δ also suggests that the process was not a simple melting of GEMS. The sintering process would have to be able to concentrate Ca which suggests that Ca was either mobilized from other material or was more abundant in the region of the nebula where the sintering occurred. This suggests a link between the oxidation process, sulfidation process, and concentration of elements such as Ca and K.

One possibility is to ascribe the Ni-rich metals in γ, ϵ and ζ to atmospheric oxidation. The hypothesis would be that the GEMS contained Fe-Ni metal with approximately chondritic composition (i.e. Fe/Ni $\approx$20) but while decelerating in Earth's atmosphere, the heating and exposure to oxygen caused the Fe to diffuse out into the surrounding silicate or be lost from the particle. However, the absence of Ni-rich metals on the surface of β argues against this. It seems likely that this surface was also exposed to air, yet it contains abundant Fe-rich metal. It also shows evidence for sintering whereas the GEMS with Ni-rich metals do not. It is unlikely that atmospheric entry caused the Fe-depletion in γ and simultaneously sintered the GEMS in β without oxidizing them. There is no obvious reason why atmospheric entry should affect the different regions differently. Some possibilities to consider are highly non-uniform gas exposure during entry, and the influence of carbonaceous coatings/ablation around GEMS. More likely, oxidation and heating processes were active in the nebula so that the regions experienced different oxidation histories. Later the regions were glued together to form a large aggregate. The small magnetite rims visible on both the GEMS with Ni-rich metals and Ni-poor metals are likely caused by atmospheric entry.

Conclusion: GEMS often show signs of significant oxidation which cannot be ascribed solely to heating and oxidation by atmospheric entry. Instead, they are diverse and either formed or were altered in environments with variable f_{O_2}, f_{S_2} and heating. This parallels our previous work showing that GEMS and GEMS-like objects experienced significant sulfidation and heating processes in the nebula. A complete understanding of the history of GEMS and equilibrated aggregates will require considering many alteration processes in the solar nebula.

Acknowledgments: NCEM is supported by the Director, Office of Energy Research, Office of Basic Energy Sciences, Materials Sciences Division of the U.S. Department of Energy, under Contract No. DE-AC02-05CH11231.

References: [1] Gainsforth, Z. *et al.* (2016). *LPSC* [2] Gainsforth, Z. *et al.* (2017). *Am. Min.*, 102(9), 1881-1893. [3] Keller, L. P., & Messenger, S. (2011). *GCA*, 75(18), 5336-5365. [4] Ishii, H. A., *et al.* (2018). *PNAS*, 115(26), 6608-6613. [5] Brownlee, D E., *et al.* (2005). *LPSC*. [6] Joswiak, D J., *et al.* (1998). *LPSC*. [7] Westphal, A J., *et al.* (2018). *arXiv*, 1805.05921. [8] Brownlee, D. E., *et al.* (2005). *LPSC*. [9] Seinfeld, J. H., & Pandis, S. N. (2016). Third Ed., Wiley. [10] , Barth, M. I. F., *et al.* (2017). *MAPS*, 53(2), 187-203.